JBC RESEARCH ARTICLE

Dual Cre and Dre recombinases mediate synchronized lineage tracing and cell subset ablation *in vivo*

Received for publication, February 14, 2022, and in revised form, April 2, 2022 Published, Papers in Press, April 21, 2022,
https://doi.org/10.1016/j.jbc.2022.101965

Haixiao Wang[1,2], **Lingjuan He**[1,3], **Yan Li**[1,2], **Wenjuan Pu**[1,2], **Shaohua Zhang**[1,2], **Ximeng Han**[1,2], **Kathy O. Lui**[4,5], and **Bin Zhou**[1,2,6,7,*]

From the [1]*State Key Laboratory of Cell Biology, Shanghai Institute of Biochemistry and Cell Biology, Center for Excellence in Molecular Cell Science, Chinese Academy of Sciences, Shanghai, China;* [2]*University of Chinese Academy of Sciences, Shanghai, China;* [3]*School of Life Science, Westlake University, Shanghai, China;* [4]*Department of Chemical Pathology, and* [5]*Li Ka Shing Institute of Health Sciences, Prince of Wales Hospital, The Chinese University of Hong Kong, Hong Kong, China;* [6]*School of Life Science and Technology, ShanghaiTech University, Shanghai, China;* [7]*School of Life Science, Hangzhou Institute for Advanced Study, University of Chinese Academy of Sciences, Hangzhou, China*

Edited by Patrick Sung

Genetic technology using site-specific recombinases, such as the Cre-loxP system, has been widely employed for labeling specific cell populations and for studying their functions *in vivo*. To enhance the precision of cell lineage tracing and functional study, a similar site-specific recombinase system termed Dre-rox has been recently used in combination with Cre-loxP. To enable more specific cell lineage tracing and ablation through dual recombinase activity, we generated two mouse lines that render Dre- or Dre+Cre-mediated recombination to excise a stop codon sequence that prevents the expression of diphtheria toxin receptor (DTR) knocked into the ubiquitously expressed and safe Rosa26 locus. Using different Dre- and Cre-expressing mouse lines, we showed that the surrogate gene reporters tdTomato and DTR were simultaneously expressed in target cells and in their descendants, and we observed efficient ablation of tdTomato$^+$ cells after diphtheria toxin administration. These mouse lines were used to simultaneously trace and deplete the target cells of interest through the inducible expression of a reporter and DTR using dual Cre and Dre recombinases, allowing a more precise and efficient study of the role of specific cell subsets within a heterogeneous population in pathophysiological conditions *in vivo*.

Recent advances in dissecting cellular heterogeneity at a single-cell resolution have identified many unappreciated cell subsets during multiple biological processes. Nevertheless, they are often poorly characterized cell populations. Targeted cell ablation would allow us to determine the scarcely understood function of a specific cell lineage *in vivo*. In addition to the conventional Cre-loxP system, Dre-rox can be used in combination with Cre-loxP for a more precise study of different cell lineages (1). Dre recombinase, orthogonal to Cre recombinase, which recognizes the rox site, was discovered in P1-like phages and yielded highly efficient recombination (2). While Cre-mediated expression of diphtheria toxin receptor (DTR) is one of the most widely used strategies for targeted cell ablation (3), there is no model employing Dre-mediated expression of DTR in mice. Diphtheria toxin (DT) is a bacterial exotoxin that targets human cells but not murine cells (4). It is a secretory single polypeptide produced from *Corynebacterium diphtheriae* and consists of two subunits, A and B (DT-A and DT -B). Its action requires the expression of DTR on living cells (5). Following cell surface binding of DT-B and receptor-mediated endocytosis of DTR, subunit A (DT-A, or DTA) translocates from the acidic late endosome to the cytosol where it ADP-ribosylates a diphthamide residue of elongation factor 2 (6, 7), terminating protein synthesis (8–11) and ultimately triggering cell death (12). Although DT-A acts on all eukaryotic elongation factor 2, murine and rat cells are insensitive to DT (13, 14). In humans and apes, which are DT-sensitive species, DTR has been identified as a membrane-anchored heparin-binding epidermal growth factor (HB-EGF)–like precursor (5). HB-EGF precursors of murine and rat cells fail to bind to DT-B and thus are not *bona fide* receptors (15), rendering them resistant to the toxin (13, 14). Accordingly, transgenic expression of DTR encoded by the simian HB-EGF precursor (*Hbegf*) in DT-resistant mouse cells would confer DT sensitivity. Here, we attempted to generate mouse lines that rendered Dre- or Dre+Cre-mediated inducible DTR expression, facilitating cell ablation in the target cells of interest.

Cre-loxP system is a powerful tool for genetic lineage tracing and cell ablation studies (16). However, the degree of recombination in cells of Rosa26-reporter or *Rosa26-iDTR* mice varies significantly between different Rosa26 alleles used as readouts (17, 18). Indeed, previous studies have also reported that fate mapping results elucidated by different Cre-mediated reporter alleles were inconsistent with the use of different Rosa26 lines (17, 19). Such discrepancies can be attributed to the varying efficiency of Cre-loxP–mediated recombination. In fact, the intervening distance between the loxP sites flanking the *Stop* fragment affects recombination efficiency (20, 21). A number of Cre lines engender inconsistent fate maps depending on the reporter lines employed, which include *Nkx2.5-Cre*, *Pcp2-Cre*, *Chat-Cre*, *Wt1-Cre*, and

* For correspondence: Bin Zhou, zhoubin@sibs.ac.cn.

Isl1-Cre (17, 18, 22–25). Different loci within the same cell may also display varying recombination efficiencies (26), suggesting that Cre-loxP recombination is position-dependent and the readout from one locus (such as Rosa26) may not be necessarily in line with that derived from a different one (such as Hprt or Hipp11) (21, 27).

Considering these limitations, it is difficult to compare fate mapping results that were generated from even the same gene promoter–mediated Cre that targeted different surrogate reporters. Similarly, it may not be correct to assume that the efficiency of lineage tracing by the same gene promoter–mediated Cre would be the same as that of cell ablation given that the recombination efficacy at one Rosa allele (*e.g.*, *Rosa26-lox-stop-lox(LSL)-Reporter)* may not be as efficient as that at another allele (*e.g.*, *Rosa26-LSL-DTR*). To circumvent this issue, we generated two Rosa26-reporter-DTR mouse lines to achieve synchronized expression of a surrogate reporter and DTR upon Dre- or Dre+Cre-mediated recombination, allowing for lineage tracing and genetic ablation of DTR-expressing cells with the same efficiency after DT administration.

Results

To enable synchronized expression of a reporter and DTR by targeting one genomic locus, we placed a "self-cleaving" 2A peptide sequence between tdTomato and DTR (Fig. 1*A*). This design would allow for simultaneous generation of tdTomato and DTR from a single transcript, enhancing efficiency by avoiding the use of an internal ribosome entry sequence and the generation of a second transcript (28). We targeted a complementary DNA (cDNA)-containing tdTomato-2A-DTR sequence in the well-characterized Rosa26 locus (29). To allow conditional expression of tdTomato and DTR, we also inserted a rox-flanked transcriptional *Stop* fragment upstream of the tdTomato-2A-DTR cDNA (Fig. 1*A*). Transcription of *R26-R-tdT-DTR* is normally blocked by the *Stop* sequence that is excised upon activation of the Dre recombinase, yielding heritable expression of tdTomato-2A-DTR in Dre^+(Dre-positive) cell lineages (30) (Fig. 1*B*). Due to the presence of a 2A sequence (31), the single *tdTomato-2A-DTR* transcript was translated as a single polypeptide that was subsequently cleaved to generate separate tdTomato and DTR proteins. Thus, DTR^+ (DTR-positive) cells simultaneously expressed tdTomato that could be potentially ablated after DT treatment (Fig. 1*C*). Genotypic characterization by PCR verified correct genetic targeting of tdTomato-2A-DTR in the murine Rosa26 locus (Fig. 1*D*). Immunostaining for tdTomato on sections of multiple organs collected from *R26-R-tdT-DTR* showed no tdTomato signal, suggesting no leakiness of this allele without recombinase-mediated recombination (Fig. 1*E*).

Next, we used an endothelial cell-specific Dre line, *Cdh5-Dre* (32), to cross with *R26-R-tdT-DTR* (Fig. 2, *A* and *B*), and examined whether tdTomato and DTR were simultaneously and specifically expressed in endothelial cells. By whole-mount epifluorescence of several organs, we detected tdTomato signals in 6-week-old *Cdh5-Dre;R26-R-tdT-DTR* mice (Fig. 2, *C* and *D*), suggesting that expression of tdTomato was only induced after Dre-rox recombination. To confirm that the tdTomato signal was confined to endothelial cells, we performed immunostaining for tdTomato, DTR, and CD31 on sections of 6-week-old *Cdh5-Dre;R26-R-tdT-DTR* mice. We found that tdTomato was specifically expressed in endothelial cells, and tdTomato colocalized with DTR in the same cells (Fig. 2*E*). Moreover, treatment with DT led to severe bleeding in the intestine of these mice (Fig. 2, *F* and *G*) that died shortly after DT treatment (Fig. 2*H*). Immunostaining for tdTomato, DTR, and CD31 shows that compromised pattern of $tdTomato^+DTR^+$ endothelial cells of intestine in DT-treated mice compared with the control (Fig. 2*I*). Altogether, these data illustrated that the *R26-R-tdT-DTR* mice could be used for tracing and depletion of specific cell populations mediated by Dre recombinase.

While Cre-loxP has been widely used in lineage tracing studies (33–35), expression of Cre recombinase in nontarget cell populations may compromise the precision of lineage tracing (36, 37). Dual recombinases using Cre and Dre would provide an alternative approach for more precise lineage tracing and gene targeting of a specific cell population (38). To enable Cre+Dre responsive DTR, we next generated a new reporter mouse line by inserting a loxP-flanked and rox-flanked transcriptional *Stop* fragment upstream of tdTomato-2A-DTR cDNA into the Rosa26 locus, combining the Cre-loxP and Dre-rox systems. We named this line as *R26-LR-tdT-DTR* (Fig. 3*A*), in which tdTomato-2A-DTR could be activated in cells that expressed both Cre and Dre after the two *Stop* cassettes being removed by Cre-loxP and Dre-rox recombination, respectively (Fig. 3, *B* and *C*). The presence of Cre or Dre recombinase alone would not result in the expression of tdTomato-2A-DTR (Fig. 3*C*). DT treatment would lead to ablation of $tdTomato^+DTR^+$ cells (Fig. 3*D*). We next examined whether the loxP-flanked or rox-flanked-*STOP* cassettes could block the expression of tdTomato-2A-DTR. To achieve this, we crossed *R26-LR-tdT-DTR* with *ACTB-Cre* (37) and *CAG-Dre* (2), respectively. ACTB is a housekeeping gene expressed in cell cytoskeleton of cell in whole organism. Immunostaining for tdTomato on sections showed no tdTomato expression in tissues collected from *ACTB-Cre;R26-LR-tdT-DTR* or *CAG-Dre;R26-LR-tdT-DTR* (Fig. 3*E*), indicating that loxP-flanked or rox-flanked *STOP* blocked the expression of tdTomato-2A-DTR. These results also demonstrated no Cre-rox or Dre-loxP recombination in our system.

To characterize the tdTomato and DTR activity in *R26-LR-tdT-DTR*, we crossed it with *ACTB-Cre* and *Tnni3-Dre* (37), which specifically target cardiomyocytes in the heart (Fig. 4*A*). In this triple knockin mouse line, *ACTB-Cre;Tnni3-Dre;R26-LR-tdT-DTR*, expression of Cre and Dre recombinases resulted in tdTomato-2A-DTR expression in $TNNI3^+$ cardiomyocytes (Fig. 4*B*). To verify whether tdTomato-2A-DTR expression and DTR function were specific to cardiomyocytes, we performed PBS or DT injection in these mice (Fig. 4*C*). We

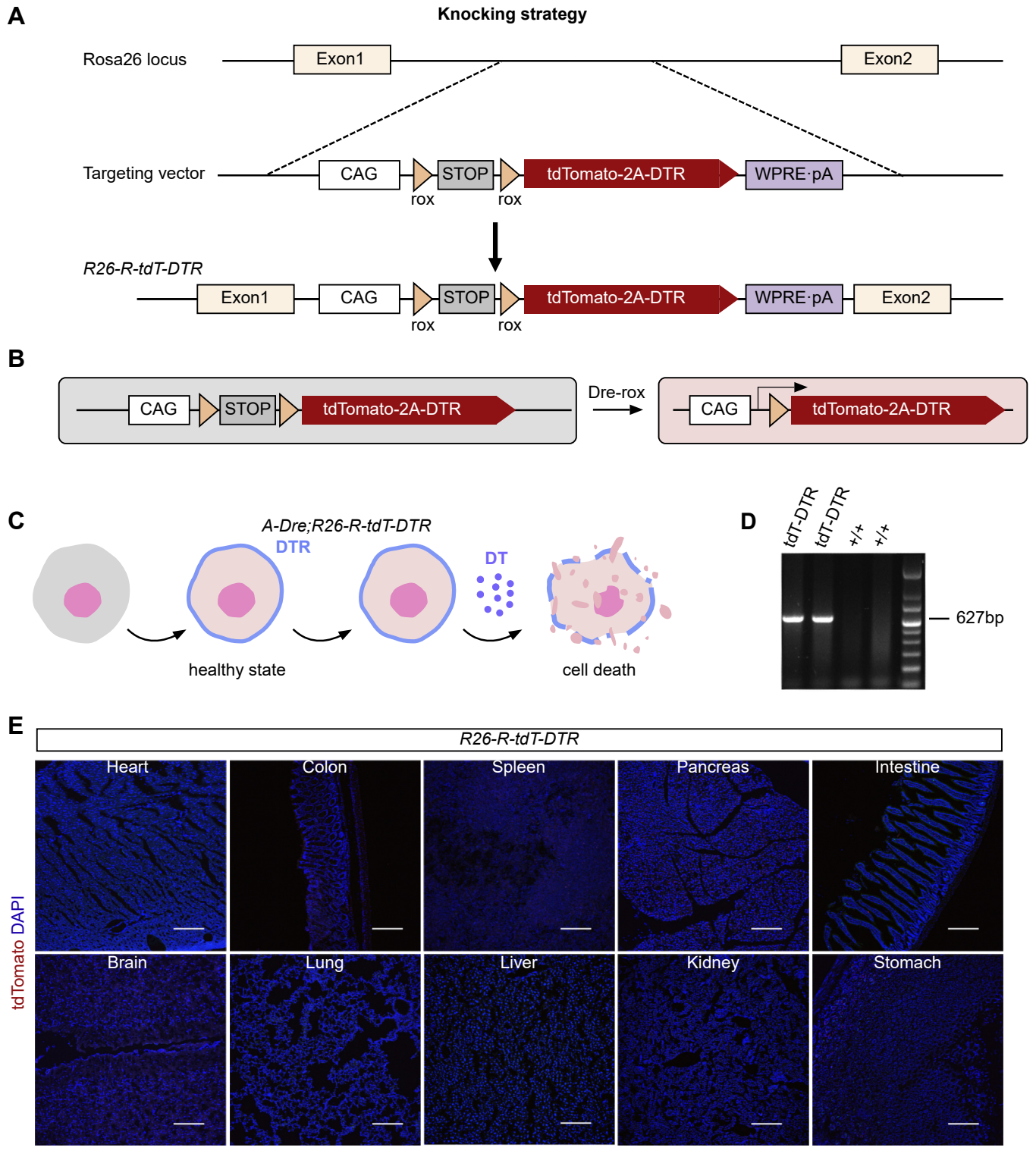

Figure 1. Generation of the *R26-R-tdT-DTR* mouse line. *A*, a schematic figure showing the gene targeting strategy for generation of *R26-R-tdT-DTR* allele. *B*, a cartoon figure showing expression of tdTomato and DTR after Dre-rox recombination–mediated removal of *Stop* cassette. *C*, a cartoon figure showing tissue-specific expression of DTR and DT-induced cell ablation. *D*, genotyping verification of *R26-R-tdT-DTR* mice by PCR. *E*, immunostaining for tdTomato shows no expression of tdTomato in *R26-R-tdT-DTR* mice. The scale bar represents 100 μm. Each image is representative of five individual biological samples. DTR, diphtheria toxin receptor; DT, diphtheria toxin.

speculated that DT treatment could lead to severe heart injury that limited the movement of the mice. Movement trajectory line results from water mazing experiments showed that the motion ability of mice treated with DT for 2 days was severely impaired compared with the PBS-treated controls (Fig. 4*D*). Echocardiographic results showed normal levels of ejection fraction and fractional shortening of DT-treated mice (data not shown) that displayed abnormal heart shape (Fig. 4, *E* and *F*).

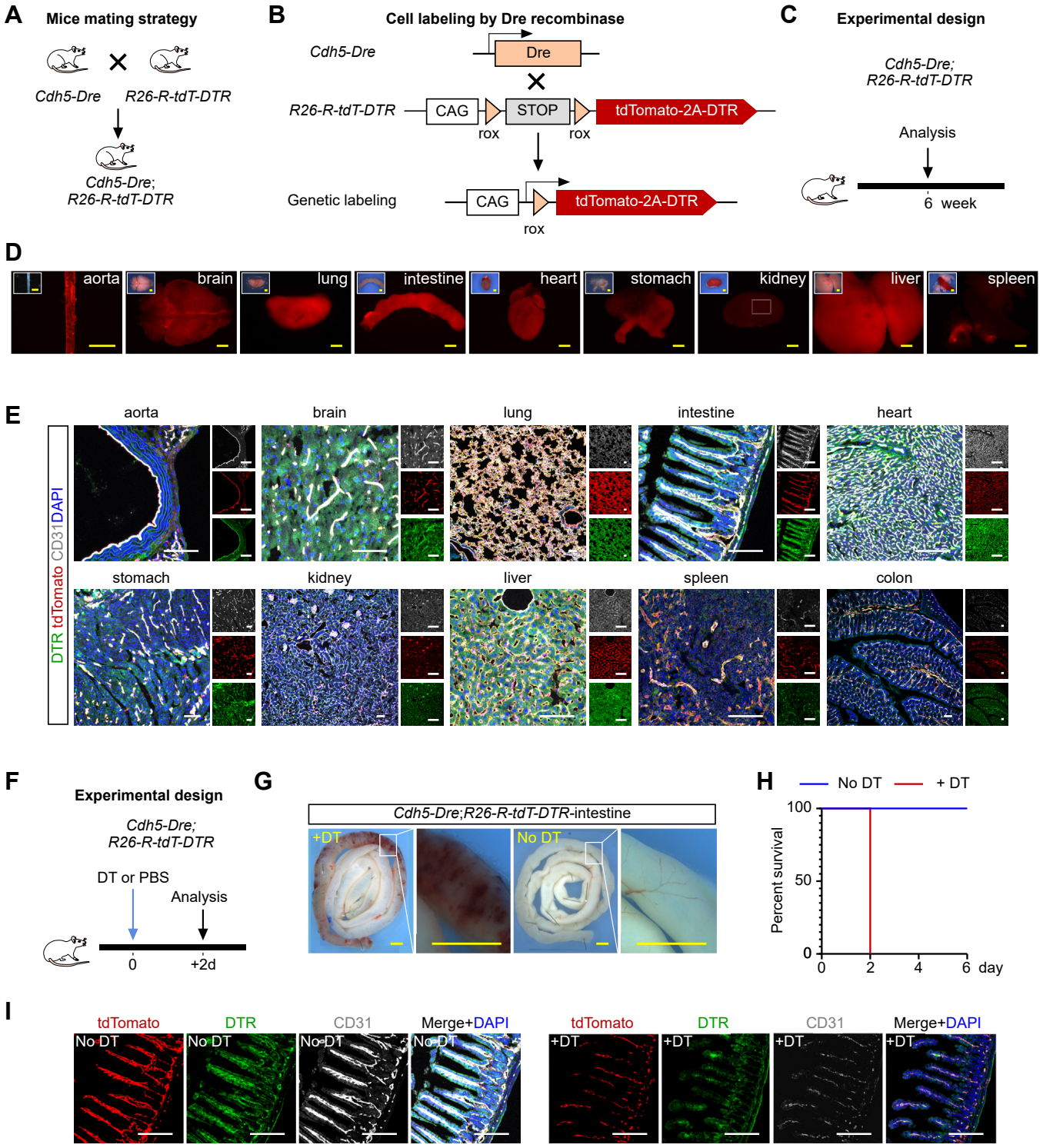

Figure 2. Expression of DTR and tdTomato in *R26-R-tdT-DTR* induced by *Cdh5-Dre*–mediated recombination. *A*, a cartoon figure showing the mating strategy of mice. *B*, a schematic figure showing the genetic recombination of the *R26-R-tdT-DTR* allele with *Cdh5-Dre*. *C*, a schematic figure showing the experimental design. *D*, whole-mount epifluorescence views of multiple organs collected from *Cdh5-Dre;R26-R-tdT-DTR* mice. *Yellow scale bar* represents 2000 μm. *E*, immunostaining for DTR, CD31, and tdTomato on sections of *Cdh5-Dre;R26-R-tdT-DTR* mice shows tdTomato and DTR expression in multiple tissues or organs. *White scale bar* represents100 μm. *F*, a schematic figure showing experimental strategy. *G*, whole-mount view of small intestine after DT or PBS treatment. *Yellow scale bar* represents 2000 μm. *H*, survival of DT treatment- and control-mice. *I*, immunostaining for tdTomato, DTR, and CD31 on intestine sections after DT or PBS treatment. *White scale bar* represents 100 μm. Each image is representative of five individual biological samples. DTR, diphtheria toxin receptor; DT, diphtheria toxin.

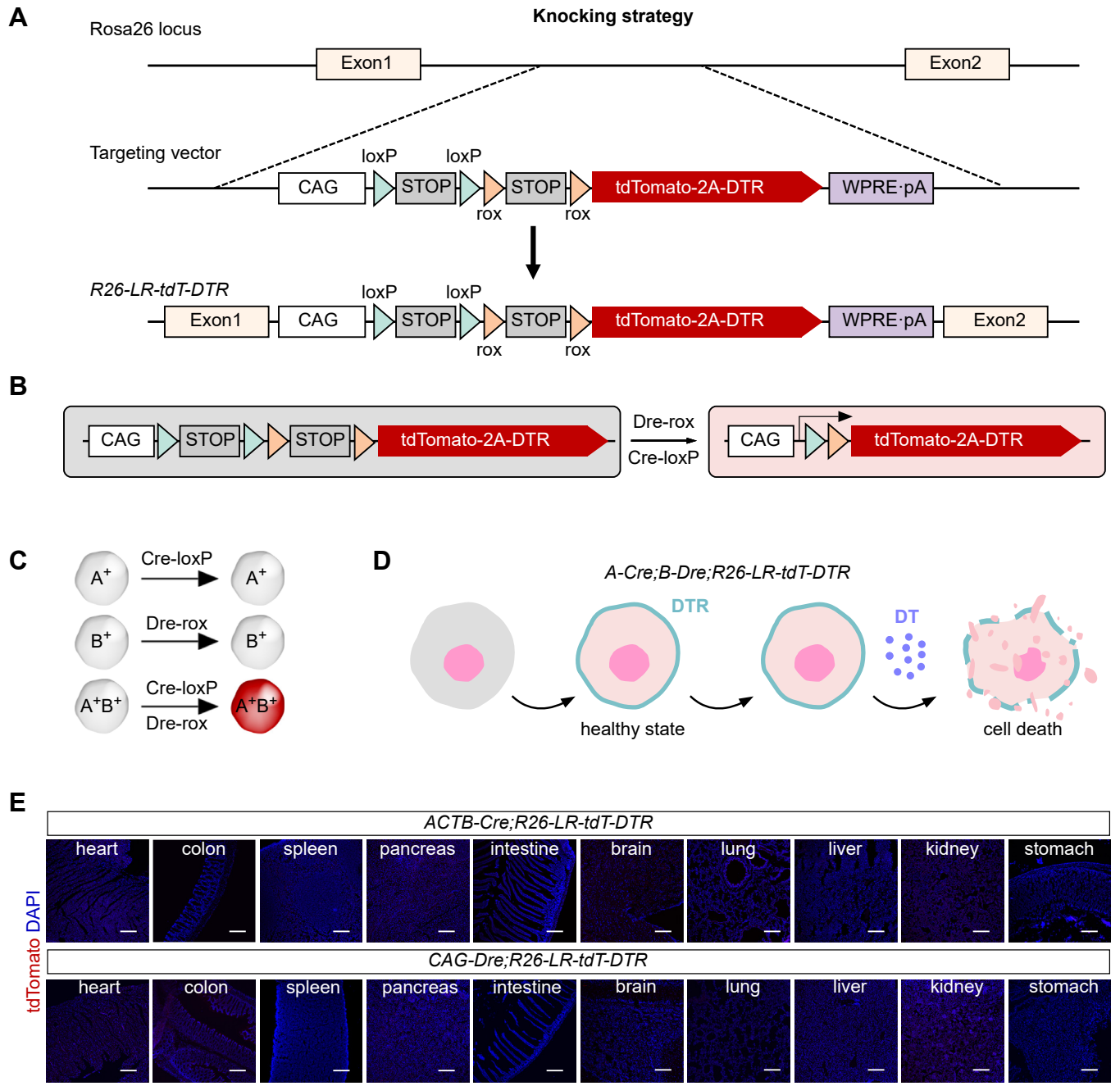

Figure 3. Generation of the *R26-LR-tdT-DTR* mouse line. *A*, a schematic figure showing the gene targeting strategy for the construction of the *R26-LR-tdT-DTR* allele. *B* and *C*, cartoon figures showing tdTomato and DTR expression after both Cre-loxP– and Dre-rox– mediated recombinations. *D*, a cartoon figure showing tissue-specific expression of DTR and genetic ablation of cells after DT treatment. *E*, immunostaining for tdTomato on sections of multiple tissues or organs collected from *ACTB-Cre;R26-LR-tdT-DTR* mice (*upper panel*) or *CAG-Dre;R26-LR-tdT-DTR* mice (*lower panel*). The scale bar represents 100 μm. Each image is representative of five individual biological samples. DTR, diphtheria toxin receptor; DT, diphtheria toxin.

Whole-mount epifluorescence imaging showed tdTomato signals in both the DT- and PBS-treated mice. Notably, tdTomato signals of the DT-treated mice were significantly weaker than those of PBS-treated controls (Fig. 4*G*). Immunostaining results further showed coexpression of DTR and tdTomato in cardiomyocytes of PBS-treated mice, with the DTR signal being located in the cell membrane while the tdTomato signal being observed in the cytoplasm (Fig. 4*H*). In DT-treated hearts, we noticed that tdTomato and DTR signals were lost in a large proportion of myocardium (Fig. 4*H*). Immunostaining for cardiac Troponin T (cTnT), a marker of cardiomyocyte (39), and tdTomato further confirmed that ablation of the tdTomato$^+$ area led to the loss of cTnT signals, indicating the specificity of cell labeling and depletion after DT treatment (Fig. 4*I*). Consistently, TUNEL assays for detection of cell necrosis revealed more apoptotic signals in the DT-treated than control hearts (Fig. 4*J*). Taken together, these data demonstrated that *R26-LR-tdT-DTR* could be used for specific labeling and

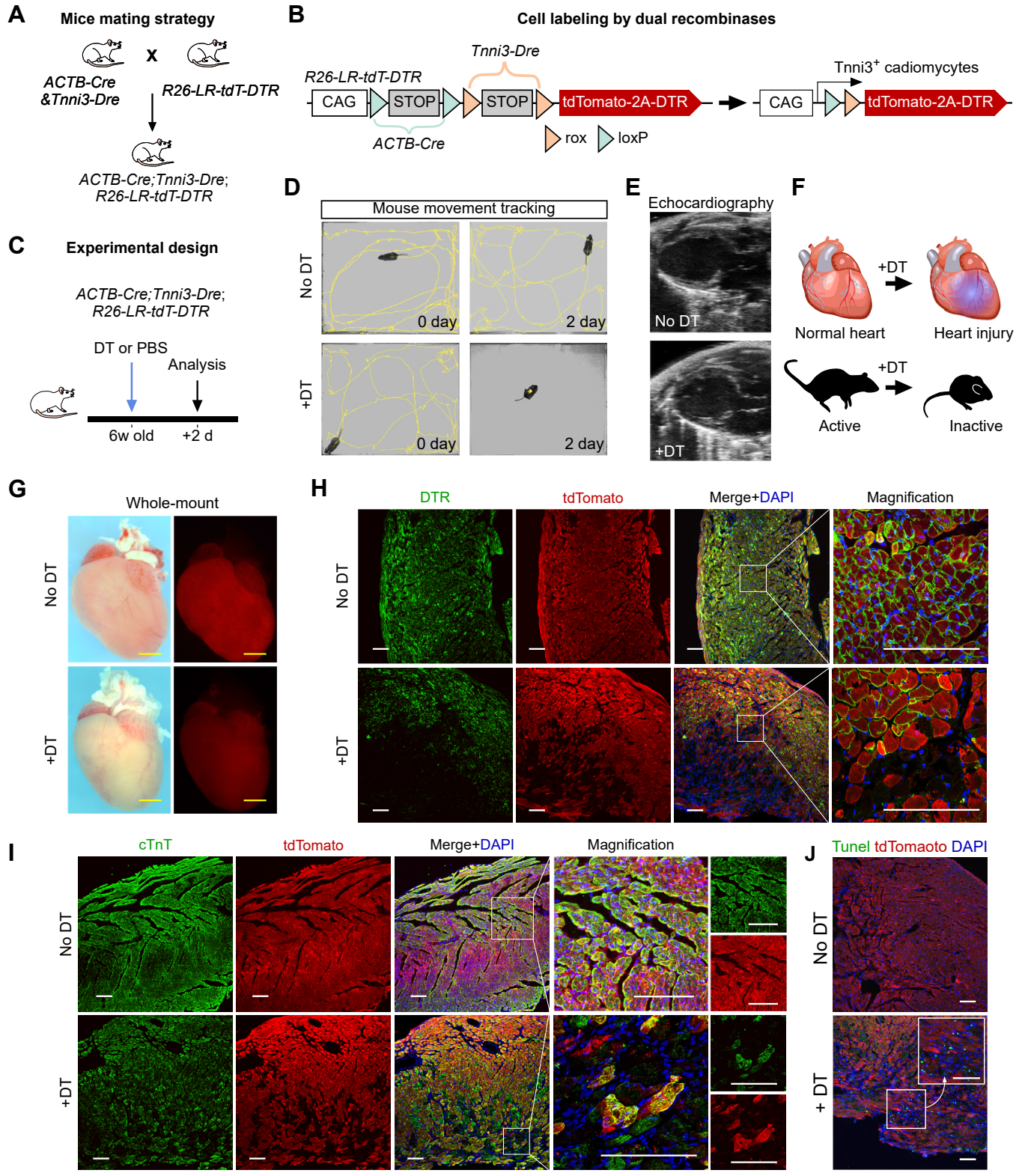

Figure 4. DTR-mediated cardiomyocyte ablation after DT administration. *A*, a cartoon figure showing the mating strategy for the generation of *ACTB-Cre;Tnni3-Dre;R26-LR-tdT-DTR* triple transgenic mice. *B*, a schematic figure showing the genetic recombination of the *R26-LR-tdT-DTR* allele with *Tnni3-Dre* and *ACTB-Cre*. *C*, a schematic figure showing experimental design. *D*, a water maze experiment for movement tracking of mice. *E*, echocardiography of mice treated with DT or PBS. *F*, a cartoon figure indicating heart injury and the inactive state of mice after DT treatment. *G*, whole-mount view of triple transgenic mice treated with PBS or DT. *Yellow scale bar* represents 2000 μm. *H*, immunostaining for DTR and tdTomato on heart sections of triple transgenic mice. *White scale bar* represents100 μm. *I*, immunostaining for cTnT and tdTomato on heart sections of triple transgenic mice. *White scale bar* represents 100 μm. *J*, immunostaining for Tunel and tdTomato on heart sections. *White scale bar* represents 100 μm. Each image is representative of five individual biological samples. DTR, diphtheria toxin receptor; DT, diphtheria toxin.

ablation of distinct cell populations using the Cre-loxP and Dre-rox systems.

Having established the *R26-LR-tdT-DTR* mouse line as a target model for constitutively active Cre and Dre, we next asked whether cell labeling and depletion can be operated in a temporal manner through inducible Cre and Dre recombinases. It is known that hepatocytes of the liver are heterogeneous, as peri-central and peri-portal hepatocytes are distinct in gene expression, cell proliferation, and function (40, 41). For example, peri-central hepatocytes express CYP2E1 (cytochrome P450, family 2, subfamily e, polypeptide 1) while peri-portal hepatocytes express Mfsd2a (42). We first tested if our system could specifically target and ablate peri-central hepatocytes in mouse. We crossed *R26-LR-tdT-DTR* with *Cyp2e1-DreER* to get a double knockin *Cyp2e1-DreER;R26-LR-tdT-DTR* mouse line. We then performed AAV8-TBG-Cre injection that specifically targeted all hepatocytes (Fig. 5, *A* and *B*). In this experimental strategy, loxP-flanked and rox-flanked *Stop* cassettes of *R26-LR-tdT-DTR* would be excised by TBG promoter–driven Cre and *Cyp2e1* promoter–driven DreER after tamoxifen-induced activation respectively, rendering tdTomato and DTR expression in Cyp2e1$^+$ hepatocytes (Fig. 5*C*). Thereafter, we compared DT- and PBS-treated mouse livers. Whole-mount epifluorescence analysis showed that tdTomato signals were detected in PBS-treated livers but not in DT-treated ones (Fig. 5*D*). Immunostaining for HNF4a, DTR, and tdTomato on PBS-treated liver sections showed that tdTomato and DTR were expressed in the majority of HNF4a$^+$ hepatocytes close to the central veins (Fig. 5, *E* and *F*), confirming the highly efficient targeting strategy by inducible recombinases. Moreover, immunostaining for CYP2E1and tdTomato on sections showed that tdTomato signals were detected in CYP2E1$^+$ peri-central hepatocytes in PBS-treated livers that were barely observed after DT treatment (Fig. 5, *G* and *H*), indicating efficient ablation by DT. TUNEL signals were detected in DT-treated mouse liver sections but not in PBS-treated controls (Fig. 5*I2*). Previous studies reported that CYP2E1 was expressed not only in the liver but also in kidneys (43, 44). Indeed, we also found that CYP2E1 was expressed not only in hepatocytes but also in E-cad$^+$ epithelial cells of the kidneys in *Cyp2e1-DreER;Rosa26-rox-stop-rox-tdTomato* (*R26-R-tdT*) mouse (Fig. 5*J*). Specific targeting of hepatocytes by AAV8-TBG-Cre ensured that loxP-flanked *Stop* would be excised in the liver but not in other organs such as the kidneys (Fig. 5, *J* and *K*). Therefore, AAV8-Cre and *Cyp2e1-DreER* removed two *Stop cassettes* in hepatocytes but one *Stop cassettes* in renal epithelial cells, ensuring tdTomato and DTR expression only in the liver (Fig. 5, *J* and *K*).

Next, we asked whether the loxP-flanked *Stop* cassette could be excised by inducible Cre recombinase. We crossed *Mfsd2a-CreER* with *R26-LR-tdT-DTR* to get the *Mfsd2a-CreER;R26-LR-tdT-DTR* double knockin mice for targeting peri-portal hepatocytes. We treated these mice with AAV8-TBG-Dre and tamoxifen to enable tdTomato and DTR expression in Mfsd2a$^+$ peri-portal hepatocytes, and with DT for ablation of tdTomato$^+$ hepatocytes (Fig. 6, *A* and *B*). The liver specific TBG promoter–driven Dre recombinase removed rox-flanked *Stop* of *R26-LR-tdT-DTR*. Tamoxifen induced the activation of *Mfsd2a-CreER* that subsequently removed loxP-flanked *Stop*, driving expression of tdTomato-2A-DTR in the Rosa26 locus (Fig. 6*C*). We next collected livers from PBS- or DT-treated mice for analysis (Fig. 6*B*). Whole-mount epifluorescence results showed that tdTomato signals were detected in PBS- but not DT-treated mouse livers (Fig. 6*D*). Immunostaining for HNF4a, DT, and tdTomato on PBS-treated livers revealed that tdTomato and DTR were expressed in hepatocytes close to peri-portal veins (Fig. 6, *E* and *F*). Highly efficient depletion of tdTomato$^+$ hepatocytes was demonstrated in the DT-treated livers compared with the PBS-treated ones (Fig. 6, *G* and *H*) and evidenced by TUNEL$^+$ signals in the DT-treated group (Fig. 6*I*). Since MFSD2A was expressed not only in hepatocytes but also in endothelial cells of the brain (42, 45), we found tdTomato$^+$PE-CAM$^+$ endothelial cells and tdTomato$^+$NeuN$^+$ neurons of the brain, as well as tdTomato$^+$E-cad$^+$ epithelial cells of the small intestine in *Mfsd2a-CreER;Rosa26-loxP-stop-loxP-tdTomato* (*R26-L-tdT*) mice (Fig. 6*J*). Furthermore, we attempted to achieve specific targeting of hepatocytes by AAV8-TBG-Dre that removed loxP-flanked *Stop* in hepatocytes but not in cells of other organs. Administration of AAV8-Dre and activation of *Mfsd2a-CreER* following tamoxifen removed two *Stop cassettes* in hepatocytes but one *Stop cassettes* in brain endothelial, brain neuronal, and intestinal epithelial cells, ensuring tdTomato and DTR expression and, therefore, depletion of tdTomato$^+$ hepatocytes (Fig. 6, *J* and *K*). Taken together, our studies provided a dual recombinases–driven inducible tdTomato-DTR system for cell type–specific tracing and elimination *in vivo*.

Discussion

In this study, we generated two reporter mouse lines, *R26-R-tdT-DTR* and *R26-LR-tdT-DTR*, for *in vivo* genetic lineage tracing and cell subset elimination simultaneously. *R26-LR-tdT-DTR* permits dual recombinases–mediated activation of reporter and DTR, enhancing the precision of genetic targeting compared with that driven by a single recombinase. We provided working examples by targeting specific subpopulations of hepatocytes, such as peri-central and peri-portal hepatocytes, through dual recombinases–mediated cell labeling and ablation. Additionally, the reporter and DTR expression in one allele not only reduced the numbers of mouse crossing to ensure incorporation of reporter and DTR into the Rosa26 locus but also facilitated clearer data interpretation with the same efficiency of labeling and depletion in the reporter$^+$DTR-expressing cells. These two mouse lines would be widely applicable to study the *in vivo* function of heterogeneous cell populations not restricted to the cardiovascular and liver research fields but also in multiple organ systems during pathophysiological development.

One effective approach to more precisely targeting a distinct cell subset is to use two marker genes to define a cell population. Taking advantage of two orthogonal recombinases Cre and Dre, we recently used the combination of the Cre-loxP and Dre-rox systems to lineage trace stem cells in lung and artery wall (35, 46), record cell proliferation in liver and heart (40, 47), trace EMT in cancer metastasis and fibrosis (48, 49),

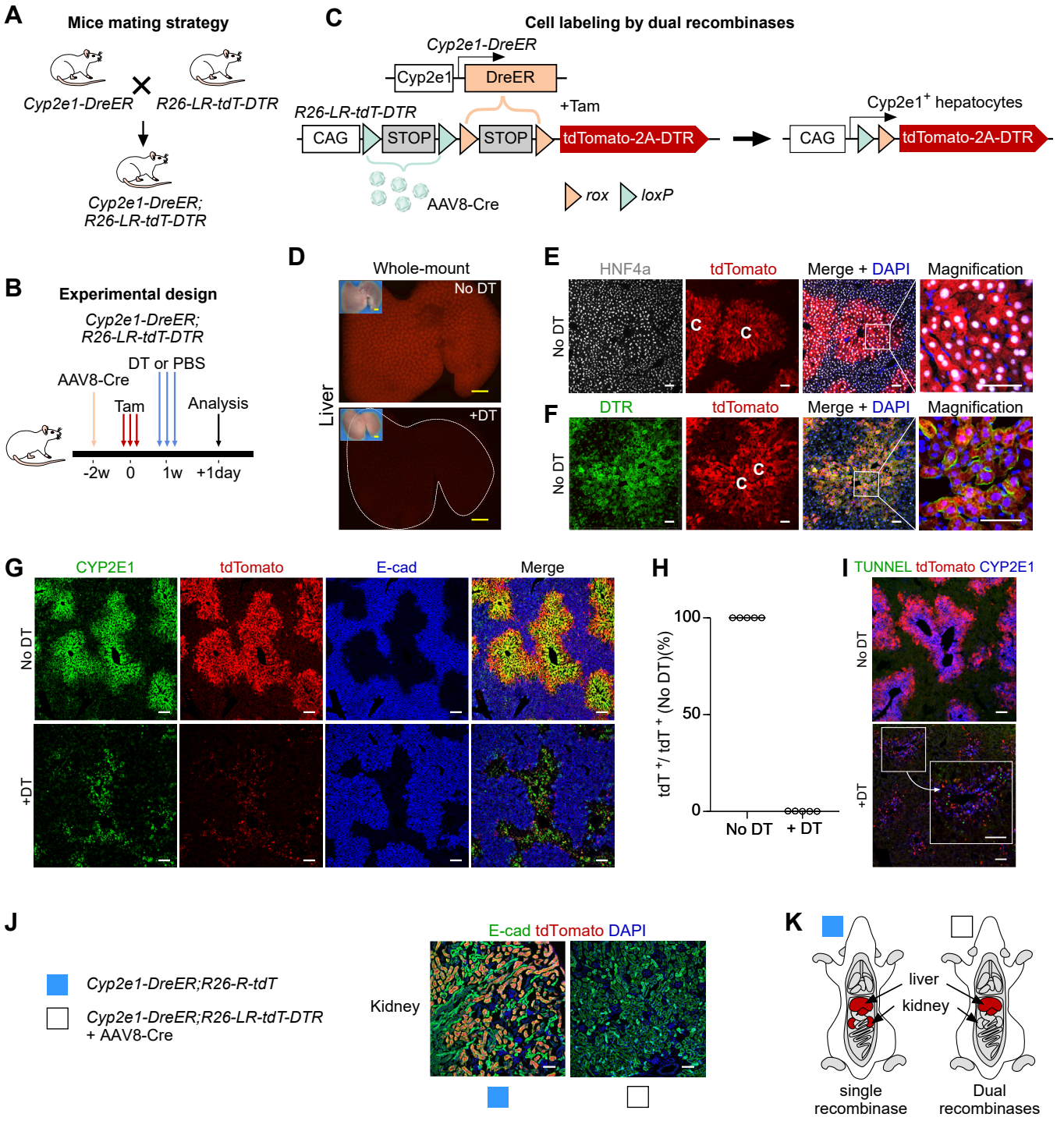

Figure 5. DTR-mediated specific ablation of Cyp2e1$^+$ peri-central hepatocytes. *A*, a cartoon figure showing the mating strategy for generation of *Cyp2e1-DreER;R26-LR-tdT-DTR* double transgenic mice. *B*, a schematic figure showing the genetic recombinations of the *R26-LR-tdT-DTR* allele with *Cyp2e1-DreER* and AAV8-TBG-Cre. *C*, a schematic figure showing experimental design. *D*, whole-mount epifluorescence view of livers collected from mice treated with DT or PBS. *Yellow scale bar* represents 2000 μm. *E* and *F*, immunostaining for tdTomato, HNF4a (E), or DTR (F) on liver sections treated with PBS. *White scale bar* represents 100 μm. C, central vein. *G*, immunostaining for CYP2E1, tdTomato, and E-cad on liver sections from mice treated with PBS or DT. *White scale bar* represents 100 μm. *H*, quantification of the percentage of tdTomato$^+$ hepatocytes (DT group) in comparison of tdTomato$^+$ hepatocytes (PBS group). *I*, immunostaining for Tunel and tdTomato on liver sections from mice treated with PBS or DT. *White scale bar* represents 100 μm. *J*, immunostaining for E-cad and tdTomato on kidney sections of *Cyp2e1-DreER;Rosa26-rox-stop-rox-tdTomato* (*R26-R-tdT*) mice and *Cyp2e1-DreER;R26-LR-tdT-DTR*. Both the mice received tamoxifen. *White scale bar* represents 100 μm. *K*, a cartoon figure showing *Cyp2e1-DreER* targeted hepatocytes specifically by using *R26-LR-tdT-DTR* mice and AAV8-TBG-Cre injection, while *Cyp2e1-DreER* targeted hepatocytes and kidney epithelial cells by using *R26-R-tdT*. Each image is representative of five individual biological samples. DTR, diphtheria toxin receptor; DT, diphtheria toxin.

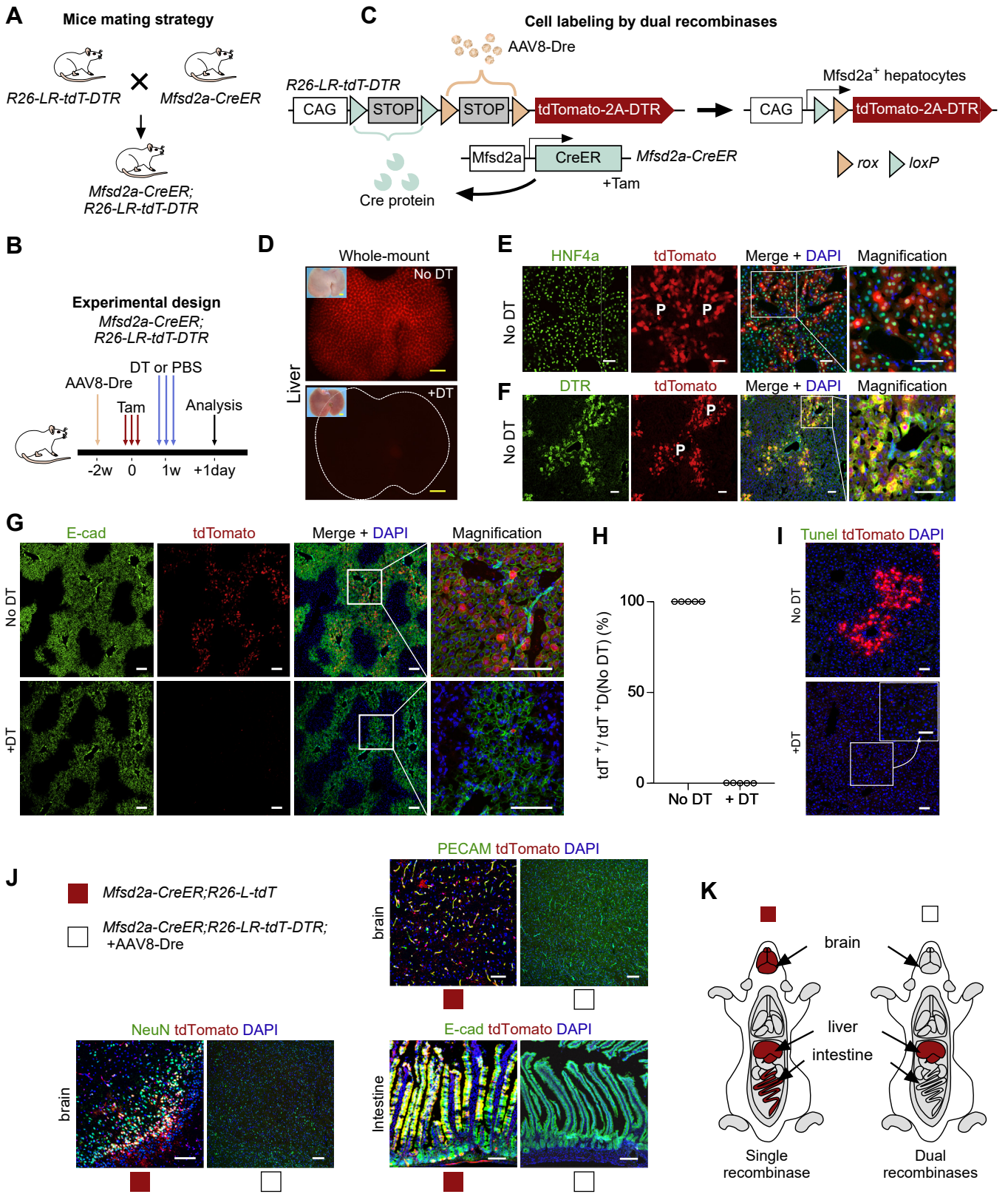

Figure 6. DTR-mediated specific ablation of Mfsd2a$^+$ peri-portal hepatocytes. *A*, a cartoon figure showing the mouse's mating strategy. *B*, a schematic figure showing the genetic recombination of the *R26-LR-tdT-DTR* allele by *Mfsd2a-CreER* and AAV8-TBG-Dre. *C*, a schematic figure showing the experimental design. *D*, whole-mount fluorescent view of livers collected from mice treated with PBS or DT. *Yellow scale bar* represents 2000 μm. *E* and *F*, immunostaining for tdTomato, HNF4a (E), or DTR (F) on liver sections of mice treated with PBS. White scale bar represents100 μm. *G*, immunostaining for E-cad and tdTomato on liver sections from mice treated with PBS or DT. *White scale bar* represents 100 μm. *H*, quantification of the percentage of tdTomato$^+$ hepatocytes (DT group) in comparison with tdTomato$^+$ hepatocytes (PBS group). n = 5. *I*, immunostaining for Tunnel and tdTomato on liver sections of mice treated with PBS or DT. *White scale bar* represents 100 um. *J*, immunostaining for PECAM, NeuN, E-cad, and tdTomato on tissue sections collected from *Mfsd2a-CreER;Rosa26-loxP-stop-loxP-tdTomato* (*R26-L-tdT*) mice and *Mfsd2a-CreER;R26-LR-tdT-DTR* mice. Both the mice received tamoxifen. *White scale bar* represents 100 μm. *K*, a cartoon figure showing *Mfsd2a-CreER*–targeted hepatocytes specifically by using *R26-LR-tdT-DTR* mice and AAV8-TBG-Dre injection, whereas *Mfsd2a-CreER*–targeted hepatocytes, brain neurons, endothelial cells, and intestine epithelial cells by using *R26-L-tdT*. Each image is a representative of five individual biological samples. DTR, diphtheria toxin receptor.

and elucidate the role of cardiac stem cells during heart repair (50, 51). Such an intersectional genetic approach has led to powerful application, assisting the understanding of cellular mechanisms during development, tissue homeostasis, regeneration, tumor growth, and metastasis (52, 53). However, the broad application of a dual recombinases–mediated genetic approach has been used for cell labeling only. To study the function of a particular cell type within a heterogeneous population, we developed the *R26-LR-tdT-DTR* mouse line driven by both Cre-loxP and Dre-rox recombination systems, rendering cells to express both tdTomato and DTR for simultaneous cell labeling and elimination. The advantage of this line is that it synchronizes the efficiency of tdTomato and DTR expression, so that tdTomato could be a faithful readout of DTR-expressing cells. As working examples, we crossed *R26-LR-tdT-DTR* with *ACTB-Cre* and *Tnni3-Dre* to excise loxP-flanked and rox-flanked *Stop* cassettes in Tnni3$^+$ cardiomyocytes. Therefore, induced cell death was only confined to DTR-expressing cardiomyocytes.

The mammalian liver has remarkable regenerative capability after injury. The hepatocytes of the liver lobule are heterogeneous in gene expression, proliferation rate, and metabolic functions (54–56). For example, peri-central hepatocytes express CYP2E1 and execute glycolysis and drug metabolism, while peri-portal hepatocytes express MFSD2A and execute gluconeogenesis and ammonia detoxification (41). Considering the distinct gene expression and functions of different hepatocyte subsets, we aimed to label these subpopulations specifically *in vivo* and eliminate them *via* DTR activation. While CYP2E1 and MFSD2A are highly enriched in peri-portal and peri-central regions of liver lobule, these genes are not only restricted to hepatocytes as their expression could also be detected in other cell types of the brain, kidneys, and intestine. We, therefore, took advantage of intersectional genetic method to genetically ablate CYP2E1$^+$ or MFSD2A$^+$ hepatocytes through Cre+Dre-mediated DTR expression in *R26-LR-tdT-DTR*. Compared with single recombinase-mediated genetic targeting, dual recombinases–mediated tracing and ablation were specific without unwanted ablation of nontarget cells outside the liver. Indeed, our results confirmed that cell death was confined to CYP2E1$^+$ or MFSD2A$^+$ hepatocytes.

In summary, we generated two novel mouse lines to ensure simultaneous expression of tdTomato and DTR operated with a synchronized efficiency driven by Dre or Cre+Dre recombinases, allowing lineage tracing and inducible ablation of a distinct cell subset within a heterogeneous population. This novel *R26-LR-tdT-DTR* mouse line could be widely used in cell models driven by dual recombinases to achieve more specific, efficient, and temporally controlled genetic targeting for studying cell function during the pathophysiological development within multiple organ systems *in vivo*.

Experimental procedures

Mouse lines

This study was carried out in strict accordance with the recommendations in the Guide for the Care and Use of Laboratory Animals of the Chinese Academy of Sciences. The protocol was approved by the Institutional Animal Care and Use Committee of the Shanghai Institute of Biochemistry and Cell Biology, Chinese Academy of Sciences. The *R26-R-tdT-DTR* and *R26-LR-tdT-DTR* mouse lines were generated by Shanghai Model Organisms and will be shared upon request.

For *R26-R-tdT-DTR* and *R26-LR-tdT-DTR*, targeting vectors were designed to contain a CAG promoter, a rox-flanked Stop fragment, and a loxP-flanked *Stop* fragment followed by a tdTomato fluorescent protein, a 2A peptide, and the simian DTR. The cassette of pCAG-rox-Stop-rox-tdTomato-2A-DTR or pCAG-loxP-stop-loxP-rox-Stop-rox-tdTomato-2A-DTR was inserted into the Rosa26 locus *via* electroporation of C57BL/6-derived embryonic stem cells. *Stop* is a Neo gene followed by multiple poly-A sequences. Correctly targeted embryonic stem cells were microinjected into C57BL/6 blastocysts. The resulting chimeric founders were crossed with WT C57BL/6 mice to generate heterozygous offsprings. For *R26-R-tdT-DTR*, in the absence of Dre, the pCAG promoter cannot drive tdTomato-2A-DTR expression due to the presence of the Stop fragment. After mating to mice carrying Dre recombinase, Dre-mediated excision results in the deletion of *Stop*, and the pCAG promoter would then drive the expression of tdTomato-2A-DTR. For *R26-LR-tdT-DTR*, the expression of tdTomato-2A-DTR requires both Cre- and Dre-mediated recombination simultaneously.

DT treatment

Six to eight week old control and *Cdh5-Dre;R26-R-tdT-DTR*, *ACTB-Cre;Tnni3-Dre;R26-LR-tdT-DTR*, *Cyp2e1-DreER;R26-LR-tdT-DTR* (AAV8-TBG-Cre injected), *Mfsd2a-CreER;R26-LR-tdT-DTR* (AAV8-TBG-Cre injected) mice were injected intraperitoneally with DT (Sigma D0564) at a dose of 10 ng/g.

Genomic PCR

We extracted genomic DNA from mouse tails. The tail tissue was lysed in a lysis buffer at 65 °C for 12 h and then centrifuged at 15,000 rpm for 8 min to obtain a genomic DNA supernatant. Next, we used isopropanol to precipitate the DNA that was washed with 70% ethanol and centrifuged at 15,000 rpm for 3 min. Finally, the DNA was dissolved in ddH_2O.

Water-maze experiment

We put the *ACTB-Cre;Tnni3-Dre;R26-LR-tdT-DTR* mice in a large box with a diagonal of 70 cm and videotaped the mice for 1 min to capture their free movements. For the control group (+PBS) and the experiment group (+DT, before DT-treatment), the mice moved randomly and continuously in the box out of curiosity. Two days after DT or PBS injection, we videotaped the mice of the control group and the experiment group for 1 min again. The DT-treated mice showed almost no movement compared to that of the control mice. After collecting videos, we imported the videos into Fiji

software (https://imagej.net/software/fiji/) for analysis. For mouse movements tracking , we used "Animal Tracker" plugin to draw motion trajectory that is indicated by yellow lines.

Echocardiograph

Anesthetized mice underwent transthoracic echocardiography using a VisualSonics' Vevo770 micro-ultrasound system (FUJIFILM VisualSonics). All measurements were performed on control and *ACTB-Cre;Tnni3-Dre;R26-LR-tdT-DTR* mice at 6 to 8 weeks old. Left ventricle ejection fraction and fractional shortening were measured as a surrogate for cardiac function.

Tissue collection and immunostaining

Immunostaining was performed according to previously described protocols (57). Briefly, mouse organs were collected in PBS on ice and then fixed in 4% paraformaldehyde at 4 °C for 1 h. After washing in PBS, tissues were treated with 30% sucrose overnight. They were then embedded in optimum cutting tissue (OCT, Sakura Finetek) and snap-frozen. Ten micrometer cryosections were collected on positively charged slides. Tissues were blocked with PBS supplemented with 0.1% Triton X-100 and 5% normal donkey serum (Jackson ImmunoResearch Laboratories, Inc) for 1 h at room temperature, followed by primary antibody incubation overnight at 4 °C. Signals were developed with Alexa fluorescent secondary antibodies (Invitrogen) and DAPI (Vector Laboratories) for nuclei couterstaining. Primary antibodies against the following proteins and dilutions were used: human HB-EGF(DTR)(AF-259-NA; 1:100, R & D systems), tdTomato(600-401-379, lot15724; 1:1000; Rockland), cTnT (Troponin I)(ab56357;1:200, Abcam), CD31(553370;1:500; BD PHharmingen), E-cadherin(AF748;1:500, R & D systems), Glutamine Synthetase (ab49873;1:1000, Abcam), tdTomato(5F8;1:100, ChromoTek), HNF4a(3113s;1:1000, Cell Signalling), CYP2E1(ab28146;1:100, Abcam), NeuN(MAB377X;1:200, Merck). Second antibodies were used: Immpress-a-goat Ig (horse) (MP-7405; 1:3, Vector Lab), Alexa donkey a-rat 647 (ab150155; 1:1000; Abcam), Alexa donkey a-goat 488 (A11055; 1:1000; Invitrogen), Alexa donkey a-rabbit 488 (A21206; 1:1000; Invitrogen), Alexa donkey a-rabbit 555 (A31572; 1:1000; Invitrogen), Alexa donkey a-goat 555 (A21432; 1:1000; Invitrogen), Alexa Fluor® 488 AffiniPure Donkey a-Goat IgG (H+L) (705-545-147; 1:1000; JIR). Images were acquired on an Olympus FV3000 confocal microscope (Olympus Corporation) and a Nikon A1 confocal microscope (Nokon Instruments Inc).

Whole-mount epifluorescence microscopy

Collected organs were washed in PBS and then placed on agar plate for whole-mount epifluorescence acquirement using the Zeiss AxioZoom V16 (Zeiss Group).

TUNEL assay

TUNEL staining was performed using the *In Situ* Cell Death Detection Kit, Fluorescein (Roche, 11684795910, Roche). Frozen tissue sections were fixed with 4% paraformaldehyde for 10 to 20 min at room temperature, washed for 30 min with PBS, and the slides were then transferred into PBS/tween (0.1% Triton X-100 in PBS) for 5 min at 4 °C. Slides were incubated with TUNEL reaction mixture for 1 h at 37 °C, and washed with PBS for 3 times. Images were acquired on an Olympus FV3000 fluorescent microscope.

Data availability

All data that support the findings of this research are provided within the article. All information is available from the corresponding author upon reasonable request.

Acknowledgments—This work was supported by Shanghai Science and Technology Commission, China (20QC1401000, 19JC1415700, 2020CXJQ01), the Program for Guangdong Introduction Innovative and Entrepreneurial Teams (2017ZT07S347), and China Postdoctoral Science Foundation, China. We thank Shanghai Model Organisms Center, Inc (SMOC) for mouse generation and institutional animal facilities for mouse husbandry.

Author contributions—H. W., S. Z., and X. H. data curation; H. W. conceptualization; H. W. methodology; H. W. software; H. W. writing–review and editing; L. H., Y. L., and W. P. supervision.

Conflict of interest—We declare that we have no financial and personal relationships with other people or organizations that can inappropriately influence our work, there is no professional or other personal interest of any nature or kind in any product, service, and/or company that could be construed as influencing the position presented in, or the review of, the article entitled.

Abbreviations—The abbreviations used are: DT, diphtheria toxin; DTR, diphtheria toxin receptor; HB-EGF, heparin-binding epidermal growth factor.

References

1. Weng, W., Liu, X., Lui, K. O., and Zhou, B. (2021) Harnessing orthogonal recombinases to decipher cell fate with enhanced precision. *Trends Cell Biol.* **32**, 324–337
2. Anastassiadis, K., Fu, J., Patsch, C., Hu, S., Weidlich, S., Duerschke, K., Buchholz, F., Edenhofer, F., and Stewart, A. F. (2009) Dre recombinase, like Cre, is a highly efficient site-specific recombinase in E. coli, mammalian cells and mice. *Dis. Model Mech.* **2**, 508–515
3. Buch, T., Heppner, F. L., Tertilt, C., Heinen, T. J., Kremer, M., Wunderlich, F. T., Jung, S., and Waisman, A. (2005) A Cre-inducible diphtheria toxin receptor mediates cell lineage ablation after toxin administration. *Nat. Methods* **2**, 419–426
4. Lee, P., Morley, G., Huang, Q., Fischer, A., Seiler, S., Horner, J., Factor, S., Vaidya, D., Jalife, J., and G, F. (1998) Conditional lineage ablation to model human diseases. *Proc. Natl. Acad. Sci. U. S. A.* **95**, 11371–11376
5. Naglich, J., Metherall, J., Russell, D., and Eidels, L. (1992) Expression cloning of a diphtheria toxin receptor: Identity with a heparin-binding EGF-like growth factor precursor. *Cell* **69**, 1051–1061
6. Draper, R. K., and Simon, M. I. (1980) The entry of diphtheria toxin into the mammalian cell cytoplasm: Evidence for lysosomal involvement. *J. Cell Biol.* **87**, 849–854
7. Sandvig, K., and Olsnes, S. (1980) Diphtheria toxin entry into cells is facilitated by low pH. *J. Cell Biol.* **87**, 828–832
8. Honjo, T., Nishizuka, Y., and Hayaishi, O. (1968) Diphtheria toxin-dependent adenosine diphosphate ribosylation of aminoacyl transferase II and inhibition of protein synthesis. *J. Biol. Chem.* **243**, 3553–3555

9. Kimata, Y., and Kohno, K. (1994) Elongation factor 2 mutants deficient in diphthamide formation show temperature-sensitive cell growth. *J. Biol. Chem.* **269**, 13497–13501
10. Robinson, E. A., Henriksen, O., and Maxwell, E. S. (1974) Elongation factor 2. Amino acid sequence at the site of adenosine diphosphate ribosylation. *J. Biol. Chem.* **249**, 5088–5093
11. Van Ness, B. G., Howard, J. B., and Bodley, J. W. (1978) Isolation and properties of the trypsin-derived ADP-ribosyl peptide from diphtheria toxin-modified yeast elongation factor 2. *J. Biol. Chem.* **253**, 8687–8690
12. Maxwell, I. H., Maxwell, F., and Glode, L. M. (1986) Regulated expression of a diphtheria toxin A-chain gene transfected into human cells: Possible strategy for inducing cancer cell suicide. *Cancer Res.* **46**, 4660–4664
13. Mekada, E., Kohno, K., Ishiura, M., Uchida, T., and Okada, Y. (1982) Methylamine facilitates demonstration of specific uptake of diphtheria toxin by CHO cell and toxin-resistant CHO cell mutants. *Biochem. Biophys. Res. Commun.* **109**, 792–799
14. Pappenheimer, A. M., Jr., Harper, A. A., Moynihan, M., and Brockes, J. P. (1982) Diphtheria toxin and related proteins: Effect of route of injection on toxicity and the determination of cytotoxicity for various cultured cells. *J. Infect. Dis.* **145**, 94–102
15. Mitamura, T., Higashiyama, S., Taniguchi, N., Klagsbrun, M., and Mekada, E. (1995) Diphtheria toxin binds to the epidermal growth factor (EGF)-like domain of human heparin-binding EGF-like growth factor/diphtheria toxin receptor and inhibits specifically its mitogenic activity. *J. Biol. Chem.* **270**, 1015–1019
16. Buckingham, M. E., and Meilhac, S. M. (2011) Tracing cells for tracking cell lineage and clonal behavior. *Dev. Cell* **21**, 394–409
17. Ma, Q., Zhou, B., and Pu, W. (2008) Reassessment of Isl1 and Nkx2-5 cardiac fate maps using a Gata4-based reporter of Cre activity. *Dev. Biol.* **323**, 98–104
18. Madisen, L., Zwingman, T., Sunkin, S., Oh, S., Zariwala, H., Gu, H., Ng, L., Palmiter, R., Hawrylycz, M., Jones, A., Lein, E. S., and Zeng, H. A. (2010) A robust and high-throughput Cre reporting and characterization system for the whole mouse brain. *Nat. Neurosci.* **13**, 133–140
19. Liu, J., Willet, S. G., Bankaitis, E. D., Xu, Y., Wright, C. V., and Gu, G. (2013) Non-parallel recombination limits Cre-LoxP-based reporters as precise indicators of conditional genetic manipulation. *Genesis* **51**, 436–442
20. Ciavatta, D., Kalantry, S., Magnuson, T., and Smithies, O. (2006) A DNA insulator prevents repression of a targeted X-linked transgene but not its random or imprinted X inactivation. *Proc. Natl. Acad. Sci. U. S. A.* **103**, 9958–9963
21. Guillot, P. V., Liu, L., Kuivenhoven, J. A., Guan, J., Rosenberg, R. D., and Aird, W. C. (2000) Targeting of human eNOS promoter to the Hprt locus of mice leads to tissue-restricted transgene expression. *Physiol. Genomics* **2**, 77–83
22. Cai, C., Liang, X., Shi, Y., Chu, P., Pfaff, S., Chen, J., and Evans, S. (2003) Isl1 identifies a cardiac progenitor population that proliferates prior to differentiation and contributes a majority of cells to the heart. *Dev. Cell* **5**, 877–889
23. Prall, O., Menon, M., Solloway, M., Watanabe, Y., Zaffran, S., Bajolle, F., Biben, C., McBride, J., Robertson, B., Chaulet, H., Stennard, F. A., Wise, N., Schaft, D., Wolstein, O., Furtado, M. B., *et al.* (2007) An Nkx2-5/Bmp2/Smad1 negative feedback loop controls heart progenitor specification and proliferation. *Cell* **128**, 947–959
24. Rudat, C., and Kispert, A. (2012) Wt1 and Epicardial fate mapping. *Circ. Res.* **111**, 165–169
25. Zhou, B., and Pu, W. T. (2012) Genetic Cre-loxP assessment of epicardial cell fate using Wt1-driven Cre alleles. *Circ. Res.* **111**, e276–e280
26. Vooijs, M., Jonkers, J., and Berns, A. (2001) A highly efficient ligand-regulated Cre recombinase mouse line shows that LoxP recombination is position dependent. *EMBO Rep.* **2**, 292–297
27. Tasic, B., Hippenmeyer, S., Wang, C., Gamboa, M., Zong, H., Chen-Tsai, Y., and Luo, L. (2011) Site-specific integrase-mediated transgenesis in mice *via* pronuclear injection. *Proc. Natl. Acad. Sci. U. S. A.* **108**, 7902–7907
28. Chan, H., V, S., Xing, X., Kraus, P., Yap, S., Ng, P., Lim, S., and Lufkin, T. (2011) Comparison of IRES and F2A-based locus-specific multicistronic expression in stable mouse lines. *PLoS One* **6**, e28885
29. Soriano, P. (1999) Generalized lacZ expression with the ROSA26 Cre reporter strain. *Nat. Genet.* **21**, 70–71
30. Alexopoulou, A. N., Couchman, J. R., and Whiteford, J. R. (2008) The CMV early enhancer/chicken beta actin (CAG) promoter can be used to drive transgene expression during the differentiation of murine embryonic stem cells into vascular progenitors. *BMC Cell Biol.* **9**, 2
31. Kim, J. H., Lee, S. R., Li, L. H., Park, H. J., Park, J. H., Lee, K. Y., Kim, M. K., Shin, B. A., and Choi, S. Y. (2011) High cleavage efficiency of a 2A peptide derived from porcine teschovirus-1 in human cell lines, zebrafish and mice. *PLoS One* **6**, e18556
32. Pu, W., Han, X., Zhang, M., Li, Y., Huang, X., He, L., and Zhou, B. (2020) Resident endothelial cells generate hepatocytes through cell fusion in adult mouse liver. *J. Genet. Genomics* **47**, 225–228
33. Baker, A. H., and Peault, B. (2016) A Gli(1)ttering role for Perivascular stem cells in blood vessel remodeling. *Cell Stem Cell* **19**, 563–565
34. Ni, Z., Deng, J., Potter, C. M. F., Nowak, W. N., Gu, W., Zhang, Z., Chen, T., Chen, Q., Hu, Y., Zhou, B., Xu, Q., and Zhang, L. (2019) Recipient c-Kit lineage cells repopulate smooth muscle cells of transplant Arteriosclerosis in mouse models. *Circ. Res.* **125**, 223–241
35. Tang, J., Wang, H., Huang, X., Li, F., Zhu, H., Li, Y., He, L., Zhang, H., Pu, W., Liu, K., Zhao, H., Bentzon, J. F., Yu, Y., Ji, Y., Nie, Y., *et al.* (2020) Arterial Sca1(+) vascular stem cells generate *de novo* smooth muscle for artery repair and regeneration. *Cell Stem Cell* **26**, 81–96.e84
36. He, L., Li, Y., Huang, X., Li, Y., Pu, W., Tian, X., Cai, D., Huang, H., Lui, K. O., and Zhou, B. (2018) Genetic lineage tracing of resident stem cells by DeaLT. *Nat. Protoc.* **13**, 2217–2246
37. He, L., Li, Y., Li, Y., Pu, W., Huang, X., Tian, X., Wang, Y., Zhang, H., Liu, Q., Zhang, L., Zhao, H., Tang, J., Ji, H., Cai, D., Han, Z., *et al.* (2017) Enhancing the precision of genetic lineage tracing using dual recombinases. *Nat. Med.* **23**, 1488–1498
38. Han, X., Zhang, Z., He, L., Zhu, H., Li, Y., Pu, W., Han, M., Zhao, H., Liu, K., Li, Y., Huang, X., Zhang, M., Jin, H., Lv, Z., Tang, J., *et al.* (2021) A suite of new Dre recombinase drivers markedly expands the ability to perform intersectional genetic targeting. *Cell Stem Cell* **28**, 1160–1176.e1167
39. Saba, Z., Nassar, R., Ungerleider, R. M., Oakeley, A. E., and Anderson, P. A. (1996) Cardiac troponin T isoform expression correlates with pathophysiological descriptors in patients who underwent corrective surgery for congenital heart disease. *Circulation* **94**, 472–476
40. He, L., Pu, W., Liu, X., Zhang, Z., Han, M., Li, Y., Huang, X., Han, X., Li, Y., Liu, K., Shi, M., Lai, L., Sun, R., Wang, Q. D., Ji, Y., *et al.* (2021) Proliferation tracing reveals regional hepatocyte generation in liver homeostasis and repair. *Science* **371**, eabc4346
41. Torre, C., Perret, C., and Colnot, S. (2011) Transcription dynamics in a physiological process: Beta-catenin signaling directs liver metabolic zonation. *Int. J. Biochem. Cell Biol.* **43**, 271–278
42. Pu, W., Zhang, H., Huang, X., Tian, X., He, L., Wang, Y., Zhang, L., Liu, Q., Li, Y., Li, Y., Zhao, H., Liu, K., Lu, J., Zhou, Y., Huang, P., *et al.* (2016) Mfsd2a+ hepatocytes repopulate the liver during injury and regeneration. *Nat. Commun.* **7**, 13369
43. Liu, H., and Baliga, R. (2003) Cytochrome P450 2E1 null mice provide novel protection against cisplatin-induced nephrotoxicity and apoptosis. *Kidney Int.* **63**, 1687–1696
44. Wang, Z., Shah, S. V., Liu, H., and Baliga, R. (2014) Inhibition of cytochrome P450 2E1 and activation of transcription factor Nrf2 are renoprotective in myoglobinuric acute kidney injury. *Kidney Int.* **86**, 338–349
45. Ben-Zvi, A., Lacoste, B., Kur, E., Andreone, B. J., Mayshar, Y., Yan, H., and Gu, C. (2014) Mfsd2a is critical for the formation and function of the blood-brain barrier. *Nature* **509**, 507–511
46. Liu, Q., Liu, K., Cui, G., Huang, X., Yao, S., Guo, W., Qin, Z., Li, Y., Yang, R., Pu, W., Zhang, L., He, L., Zhao, H., Yu, W., Tang, M., *et al.* (2019) Lung regeneration by multipotent stem cells residing at the bronchioalveolar-duct junction. *Nat. Genet.* **51**, 728–738
47. Liu, X., Pu, W., He, L., Li, Y., Zhao, H., Li, Y., Liu, K., Huang, X., Weng, W., Wang, Q. D., Shen, L., Zhong, T., Sun, K., Ardehali, R., He, B., *et al.* (2021) Cell proliferation fate mapping reveals regional cardiomyocyte cell-cycle activity in subendocardial muscle of left ventricle. *Nat. Commun.* **12**, 5784

48. Li, Y., Lv, Z., Zhang, S., Wang, Z., He, L., Tang, M., Pu, W., Zhao, H., Zhang, Z., Shi, Q., Cai, D., Wu, M., Hu, G., Lui, K. O., Feng, J., *et al.* (2020) Genetic fate mapping of transient cell fate reveals N-cadherin activity and function in tumor metastasis. *Dev. Cell* **54**, 593–607.e595
49. Zhang, S., Li, Y., Huang, X., Liu, K., Wang, Q. D., Chen, A. F., Sun, K., Lui, K. O., and Zhou, B. (2021) Seamless genetic recording of transiently activated mesenchymal gene expression in endothelial cells during cardiac fibrosis. *Circulation* **144**, 2004–2020
50. He, L., Han, M., Zhang, Z., Li, Y., Huang, X., Liu, X., Pu, W., Zhao, H., Wang, Q. D., Nie, Y., and Zhou, B. (2019) Reassessment of c-Kit(+) cells for cardiomyocyte contribution in adult heart. *Circulation* **140**, 164–166
51. Li, Y., He, L., Huang, X., Bhaloo, S. I., Zhao, H., Zhang, S., Pu, W., Tian, X., Li, Y., Liu, Q., Yu, W., Zhang, L., Liu, X., Liu, K., Tang, J., *et al.* (2018) Genetic lineage tracing of nonmyocyte population by dual recombinases. *Circulation* **138**, 793–805
52. Jin, H., Liu, K., and Zhou, B. (2021) Dual recombinases-based genetic lineage tracing for stem cell research with enhanced precision. *Sci. China Life Sci.* **64**, 2060–2072
53. Liu, K., Tang, M., Jin, H., Liu, Q., He, L., Zhu, H., Liu, X., Han, X., Li, Y., Zhang, L., Tang, J., Pu, W., Lv, Z., Wang, H., Ji, H., *et al.* (2020) Triple-cell lineage tracing by a dual reporter on a single allele. *J. Biol. Chem.* **295**, 690–700
54. Cunningham, R. P., and Porat-Shliom, N. (2021) Liver zonation - revisiting old questions with new technologies. *Front. Physiol.* **12**, 732929
55. Jungermann, K., and Kietzmann, T. (1996) Zonation of parenchymal and nonparenchymal metabolism in liver. *Annu. Rev. Nutr.* **16**, 179–203
56. Ma, R., Martinez-Ramirez, A. S., Borders, T. L., Gao, F., and Sosa-Pineda, B. (2020) Metabolic and non-metabolic liver zonation is established non-synchronously and requires sinusoidal Wnts. *Elife* **9**, e46206
57. Tian, X., Hu, T., Zhang, H., He, L., Huang, X., Liu, Q., Yu, W., He, L., Yang, Z., Zhang, Z., Zhong, T. P., Yang, X., Yang, Z., Yan, Y., Baldini, A., *et al.* (2013) Subepicardial endothelial cells invade the embryonic ventricle wall to form coronary arteries. *Cell Res.* **23**, 1075–1090